Dynamics of water droplet on a heated nanotubes surface

Seol Ha Kim,[1] Ho Seon Ahn,[2,a)] Joonwon Kim,[3] Massoud Kaviany,[1,4] and Moo Hwan Kim[1,a)]
[1]*Division of Advanced Nuclear Engineering, POSTECH, Pohang 790-784, South Korea*
[2]*Division of Mechanical System Engineering, Incheon National University, Incheon 406-772, South Korea*
[3]*Department of Mechanical Engineering, POSTECH, Pohang 790-784, South Korea*
[4]*Department of Mechanical Engineering, University of Michigan, Ann Arbor, Michigan 48109, USA*

(Received 13 March 2013; accepted 16 May 2013; published online 10 June 2013)

This study investigated an effect of nanotubes on a heated surface onto Leidenfrost droplet through high speed visualization and momentum balance analysis. Delayed cutback phenomena and Leidenfrost Point (LFP) by dramatically high heating level were observed, and it is elucidated through wettable and spreadable features induced by nanotubes. As much delayed LFP, transient boiling regime with explosion-like dynamics of a water droplet on the nanotubes was observed. Furthermore, nanotubes required higher wall temperature to maintain non wetting cushion, due to the induced slip condition by porous features. © *2013 AIP Publishing LLC*.
[http://dx.doi.org/10.1063/1.4809944]

Film boiling results when a surface is significantly hotter than the liquid's boiling point, and it generates a thin of vapor layer. In case of a water droplet as a liquid, it may hover on the vapor layer by strong vaporization at vapor-liquid interface called Leidenfrost effect. As film boiling incipience for a liquid droplet, Leidenfrost Point (LFP) results in a dramatic deterioration of heat transfer performance due to the thermally insulating vapor layer, and a longer time for evaporation of a droplet is required above the LFP. Therefore, a higher LFP is important for rapid cooling of overheated components of high-power density thermal systems, such as nuclear reactors exposed in hypothetical accident condition.

Recent widespread dynamic developments in the field of nanotechnology have included promising techniques in heat transfer engineering. In particular, there have been numerous studies of the effect of nanostructures on two-phase heat transfer, such as the pool boiling heat transfer and critical heat flux (CHF).[1–7] However, only a few studies have been devoted to analyzing nanoscale effects on film boiling at high surface temperatures well over the nucleate boiling and CHF regions. Furthermore, traditional LFP models[8,9] based on hydrodynamic instability of a vapor film cannot adequately explain LFP delay due to the nanofluids deposited on the surface.[10,11] Recently, Kim *et al.*[12] reported delayed LFP due to heat conduction in thin vertical liquid filaments between water droplets and a treated surface while varying surface parameters, such as surface roughness, wettability, and nano porosity. In the present study, we investigate the effect of nanotubes on behavior and cooling performance of the water droplet on wide heating range, even much higher than the LFP. In addition, we propose a reliable mechanism for delayed LFP and stable film boiling point (initial non-wetting points), based on the water–solid interaction and nanotubes surface morphology.

The nanotubes were fabricated on a zircaloy surface (25 mm · 15 mm · 0.7 mm) via the anodic oxidation technique with hydrofluoric acid 0.5%, as reported Ahn *et al.*[13] Figures 1(a) and 1(b) show a top view and an enlarged view of the nanotubes surface, respectively. The nanotubes had an average diameter of 20 ± 3 nm and an average height of 2.52 ± 0.31 μm throughout the top and oblique (45°) views shown in Figures 1(b) and 1(c). The nanotube arrays exhibited super hydrophilic wetting (complete wetting), with a measured contact angle of $4.2° \pm 2.3°$, as shown in Figure 1(d). As the prepared surface has a nanoscale morphology consisting of tube bundles, it exhibits capillary wicking and liquid spreading on the surface via the well-known Wenzel effect.[14] A water droplet of 6 μl was vertically dispensed from a height of 10 mm (Weber number = 3.27) above the test surface, which was heated by conduction from a large brass block. After the water droplet was dispensed, its motions were captured by a high-speed camera at 5000–30 000 frames per second. The wall temperature of the test samples was measured by a K thermocouple with a diameter of 0.001 in. And the evaporation times of droplet along the increased heating level of the test surface also were measured, and it is shown in Figure 2. Generally, the LFP is determined by a jump in the evaporation time. Here, the temperature corresponding to the longest evaporation time after the jump is the LFP, thus the LFP is 300 °C on the

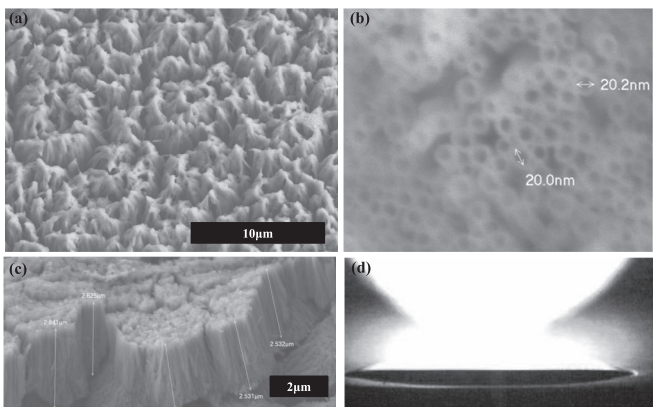

FIG. 1. Test surface with zirconium nanotubes: (a) SEM image of nanotubes, (b) enlarged view of nanotubes, (c) oblique view of nanotubes, (d) contact angle (~4.2°) between the nanotubes and a 2-μl water droplet (the contact angle with bare zirconium is ~42°).

a)Corresponding authors: hsahn@incheon.ac.kr and mhkim@postech.ac.kr

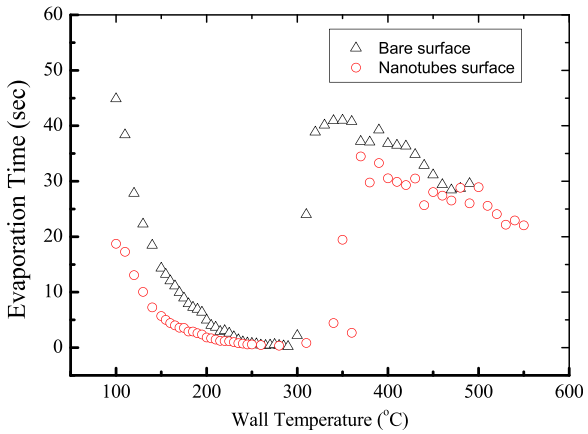

FIG. 2. Droplet (6 μl) evaporation time on each of the surfaces. Black triangles indicate the bare (untreated) surface and red circles indicate the nanotube surface.

bare surface and 370 °C on the nanotubes surface. The LFP for the bare surface is close to values previously reported in the literature. Furthermore, the evaporation time for the nanotubes surface before the LFP (~300 °C) is less than that of the bare surface, due to liquid spreading on the nanotubes surface. The dispersed water on the nanotubes surface creates a thinner liquid layer, and develops thermal conditions for evaporation more rapidly than on a bare surface. Hence, the thinner water layer evaporates at the liquid–vapor interface, or undergoes more heterogeneous nucleate boiling at the liquid–nanotube interface, leading to better cooling performance via faster evaporation.

According to Figure 2, the bare surface has almost no transient region between the CHF (minimum evaporation time) and LFP, whereas the nanotubes surface has a 70 °C transient region, which is equal to the amount of LFP delay. Figures 3(a) and 3(c) show snapshots of water droplet dynamics in the transient region (~350 °C), clearly indicating the differing behaviors of water droplets on the nanotubes and bare surfaces. The meniscus of a droplet on the bare surface is lifted up by a rapid vaporization at a recoiling triple line, a cutback phenomenon introduced by Kandlikar and Steink.[15] On the bare surface, the droplet rebounds with a cutback phenomenon and makes no further contact with the wall. It loses its downward inertia and hovers over the surface at the onset of the LFP (see the supplementary

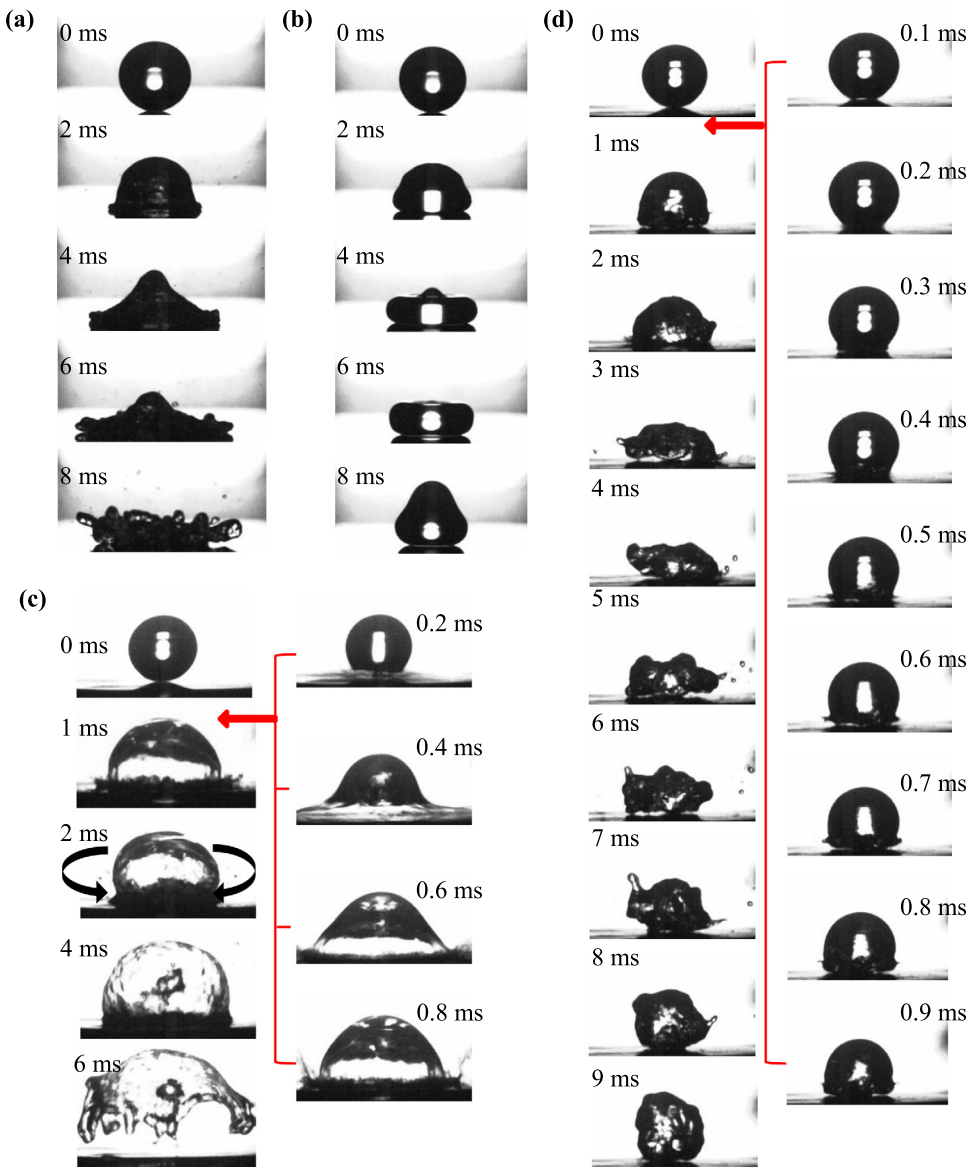

FIG. 3. Behavior of water droplets on the heated bare and nanotube surfaces. Bare surface (a) at a wall temperature of 350 °C a cutback phenomenon at 7–9 ms. (b) At a wall temperature of 450 °C, Nano surface (c) at a wall temperature of 350 °C on the nanotube surface, explosive water droplet dynamics (d) at a wall temperature of 450 °C, a cutback phenomenon at 2–4 ms, and small liquid filaments beneath the water droplet at 0.6 ms.

video[30]). However, a water droplet on the nanotubes surface is scattered into many sub-droplets, destroying the droplet interface. The meniscus spreads and many small droplets are explosively ejected in the transient region (see the supplementary video[30]). Furthermore, the wall temperature at which a droplet cannot touch the wall and results immediate rebound (the "cannot touch the wall point") is 450 °C for the bare surface and 570 °C for the nanotubes surface (see the supplementary videos[30]). In summary, the following nanotube effects on droplet dynamics and cooling were observed in this experiment: (1) fast evaporation, (2) cutback phenomena delay, (3) explosive behavior in the transient region, and (4) "cannot touch the wall point" delay. We would like to interpret the upper findings through the mechanisms of heat transfer and induced force on the nanotube surface.

First, we consider the cutback phenomenon for the water droplet on the heated bare and nanotube surfaces, as shown in Figures 3(a) and 3(d) (corresponding to bare and nanotubes surfaces with wall temperatures of 350 °C and 450 °C, respectively). The intense evaporation at the interface near a triple line exerts a vapor recoil force, which pushes the interface underneath the droplet. If the evaporation induced vapor recoil force is exerted on the water droplet weight and surface tension force holding the surface, the triple line of droplet will be recoiled and lifted as shown in Figure 3(a) at 8 ms. Since the interfacial phenomena are in motion due to evaporation at the triple line, dynamic wetting (receding contact angle) is considered as main parameters under these conditions. The improved wettability (from 49.3° to 4.3°) and the liquid dispersal phenomenon due to capillary suction between the nanostructures[16,17] bring a smaller interfacial curvature γ, and increase the surface tension $F_S = \sigma/\gamma$, where σ is surface tension of the liquid. As previously mentioned, the cutback phenomena is triggered by evaporation recoil force larger than the surface tension force. The evaporation recoil force can be evaluated by recoiling pressure, $F_V \sim P_V = \eta \cdot (\rho_v^{-1} - \rho_l^{-1})$ due to disparate densities of the vapor and liquid phase, where η is evaporation rate per area and time, determined by heat transfer amount.[18] From another perspective, the heat transfer, solution for an evaporating liquid meniscus on a heated surface was investigated by Wang *et al.*,[19] showing that the higher wall temperature, the larger heat transfer. Therefore, vapor recoiling induced by evaporation process increases with wall temperature, and a higher wall temperature is required to overcome the increased surface tension force of nanotubes. In addition, Sefiane *et al.*[20] reported that improved wettability delays recoil instability, based on an analytical and experimental investigation. Due to the rapid evaporation of vapor in a liquid meniscus, increased vapor recoil force causes recoil instability. However, if the contact angle is lower, the liquid system becomes more stable, and evaporation of wettable and dispersed water seems to be more stable. So, the more stable liquid meniscus by nanotubes endured the stronger evaporation recoil force at the higher wall superheat due to the improved wettability and liquid dispersal capability.

Next, we examine the explosive behavior of the water droplet on nanotubes surface comparing the droplet behaviors on the bare surface at 350 °C shown in Figures 3(c) and 3(a), respectively. On the bare surface, there is no explosive behavior, and short stable dispersion continues with cutback phenomenon. On the other hand, an explosive reaction occurs on the nanotubes surface; when the water droplet touches the surface, the interface is rapidly enlarged by evaporation. Liquid spreading due to nanotubes surface induces a faster movement of the liquid precursor on to the thin liquid layer than on the contact line, which implies high-speed liquid absorption in the nanostructures, as it touches the surface. The precursor line of the water droplet is already larger relative to the thin layer, and the heat transfer area of the heated wall is enlarged. Furthermore, many of pore by nanotubes contribute a number of chances of nucleate boiling as cavities. Due to the vigorous nucleate boiling by the thin layer, the falling water droplet is torn apart from the bottom as it touches the nanotubes surface. Thus, the shape of the water droplet is changed to that of a dome, while contact is maintained between the edge of the droplet and the nanotubes surface. A vaporized space forms between the dome-shaped water droplet and the nanotubes surface, as shown in the 0.2–0.6 ms segment of Figure 3(c), seems explosive. Furthermore, according to Dhir and Liaw[21] and Berenson,[22] the surface roughness and clearness (hydrophilic defects) can help the large portion of nucleate boiling during the transition boiling, thus the surface factors such as nanotubes play a role as the disturbance, which induces the instability at the interface of vapor-liquid phases.

Finally, we examine the "cannot touch the wall point" of the bare surface (see Figure 3(b)). When the water droplet approaches the bare surface at a wall temperature of 450 °C, it rebounds from the vapor cushion. On the nanotubes surface at the wall temperature of 450 °C, the droplet first contacts the surface and then hovers unstably over the surface with many of liquid filaments shown in Figure 3(d). The "cannot touch the wall point" for the nanotubes surface occurs at a wall temperature of 570 °C. We checked the vapor cushioning capability in both cases (each at the appropriate temperature) via a simple momentum balance, measuring several droplet parameters (see Figures 4(a) and 4(b)). Since both the bare (450 °C) and nanotubes surfaces (570 °C) have the same Weber number, equal measure of rebound (3.77 ± 0.025 mm), and amount of rebound time (Δt, 12.3 ± 0.2 ms), the amount of vapor cushioning force acts on the water droplets in both cases ($I = F \cdot \Delta t$, where I is the impact (momentum change) and F is the vapor cushioning force). Furthermore, the downward-facing areas (A, 2.54 ± 0.025 mm^2) of the droplets are identical and thus the same amount of vapor pressure (P) and cushioning capability are exerted. ($P = F/A$). The cushioning vapor flow is generated by the evaporation of the water droplet, known as evaporation recoil force. Biance *et al.*[23] expressed the evaporation rate of a hovering liquid droplet ($\dot{m}$) in terms of the conduction heat transfer (q_k) across the vapor cushion thickness (e) as follows:

$$\dot{m} = \frac{k_v}{h_{lv}} \frac{T_{wall} - T_{sat}}{e} \pi \lambda^2, \tag{1}$$

where k and λ are the conductivity of the vapor and the radius of the downward-facing droplet surface. Here, it is implied that a higher temperature on nanotubes surface is

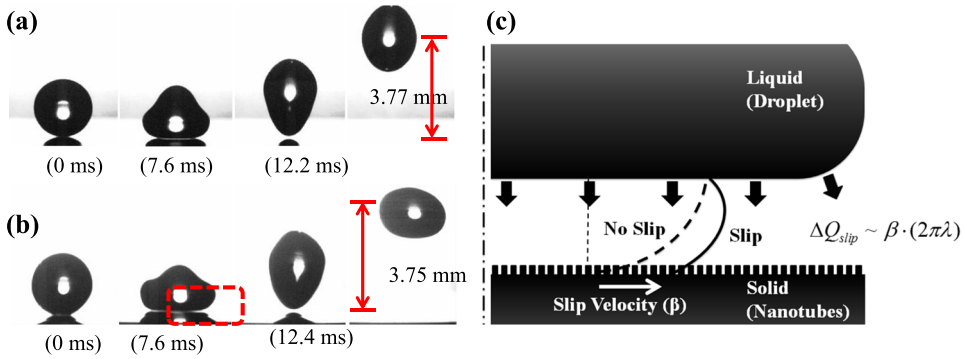

FIG. 4. "Cannot touch the wall points" for (a) the bare surface (450 °C) and (b) the nanotube surface (570 °C). At 7.6 ms, the water droplet becomes most deformed and closed to the surface. In both cases, the third image indicates the rebound time and the last image indicates the maximum rebound height. (c) Diagram of a hovering water droplet at the instant of rebound. (Red dashed rectangular in ((b), 7.6 ms)) The hovering water droplet experiences evaporation according to the vapor film thickness *e*. The slip condition of the nanotube surface induces a more effective volumetric flow rate, while reducing the cushioning performance of the vapor film.

required to obtain same vapor pressure for levitating water droplet. In order to explain the nanotubes effects, the state of a hovering water droplet on the nanotubes surface, shown in Figure 4(c), is considered. Figure 4(c) describes the radial vapor flow under the evaporated droplet and the amount of pressurized vapor acting as a cushion. Furthermore, at the "cannot touch the wall point," the vapor flow disperses radially with the continuous vapor flow, at the liquid-vapor interface side, and it induces recoil force. In terms of the hydrodynamic analysis of vapor flow near the nanotubes, if there is nanoscale roughness contacting the vapor flow, a boundary slip condition is induced.[24–26] Avedisian and Koplik[26] carried out the experimental study of Leidenfrost droplet on microscaled-porous/ceramic surfaces and showed that a portion of vapor flow from evaporation passes through porous media and slip velocity on the porous medium surface. In other words, the nano porous features of the surface create a slip condition, resulting from the vapor flow over the porous medium.[27] The slip effect of the wall ($u_{wall} = \beta$) can be expressed in terms of the gas kinetics of the porous medium (R_O), as follows:

$$\beta = \frac{8}{3\rho_v} R_0 \sqrt{\frac{\pi M}{2RT_{wall}}} \frac{\Delta P}{l}, \tag{2}$$

where M is the molecular weight, R is the gas constant, and ΔP is the pressure drop across the capillary length (l). This vapor flow slip also occurs when the substrate is porous. This has been treated with the Brinkman hydrodynamic interfacial condition[28] and the results show the same linear variation of the slip velocity with the length scale of porous medium. Based on the Carman-Kozeny relation, characteristic length scale of nanotubes (10-100 nm) can be predicted by 20 nm (diameter) of fibers, which disordered arrays as a porous media.[29] The slip velocity on the nanotubes surface (β_{nano}) is approximately O(10^{-4})m/s with the above approach, and the slip effect on the nanotubes surface (neglecting the slip effect on the bare surface affects the vapor flow rate beneath the water droplet with the following relation.

$$Q_{nano} - Q_{bare} \sim \beta_{nano} \cdot (2\pi\lambda). \tag{3}$$

Thus, nanotubes surface with a slip effect can radially disperse more vapors while retaining less vapor acting as a cushion. Consequently, in order for the "cannot touch the wall point" to be reached, a nanotubes surface requires more vapor generation through heat conduction at higher wall temperatures (Eq. (1)). Since we measured the vapor film thickness from the visualization (see Figures 4(a) and 4(b) at 7.6 ms) and other droplet parameters, we calculated that the evaporation rate for the nanotubes surface at 570 °C (0.39 mg/s) was 1.26 times larger than the evaporation rate for the bare surface (0.49 mg/s) at 450 °C. In conclusion, the slip velocity caused by the nanotubes helps the efficient escape of vapor flow beneath droplet and reduces the vapor cushion ability. Thus, higher heating level of wall which can generate more evaporation of water to vapor is required to "cannot touch the wall point" with stable film boiling in the nanotubes.

This work was supported by the National Research Foundation of Korea (NRF) grant funded by the Korea government (MSIP) (2012R1A2A1A01003376). This work was also supported by the World-class University (WCU) program of the NRF, funded by MEST (R31—30005).

[1]J. A. Eastman, S. U. S. Choi, S. Li, W. Yu, and L. J. Thompson, Appl. Phys. Lett. **78**, 718 (2001).
[2]S. M. You, J. H. Kim, and K. H. Kim, Appl. Phys. Lett. **83**, 3374 (2003).
[3]S. J. Kim, I. C. Bang, J. Buongiorno, and L. W. Hu, Appl. Phys. Lett. **89**, 153107 (2006).
[4]H. D. Kim and M. H. Kim, Appl. Phys. Lett. **91**, 014104 (2007).
[5]C. Li, Z. Wang, P.-I. Wang, Y. Peles, N. Koratkar, and G. P. Peterson, Small **4**, 1084–1088 (2008).
[6]R. Chen, M.-C. Lu, V. Srinivasan, Z. Wang, H. H. Cho, and A. Majumadar, Nano Lett. **9**(2), 548 (2009).
[7]H. J. Jo, S. H. Kim, H. Kim, J. Kim, and M. H. Kim, Nano. Res. Lett. **7**, 242 (2012).
[8]P. J. Berenson, J. Heat Transfer **83**, 351 (1961).
[9]R. E. Henry, AIChE Symp. Ser. **70**(138), 81–90 (1974).
[10]H. Kim, G. DeWitt, T. McKrell, J. Buongiorno, and L.-W. Hu, Int. J. Multiphase Flow **35**, 427 (2009).
[11]H. Kim, J. Buongiorno, L.-W. Hu, and T. McKrell, Int. J. Heat Mass Transfer **53**, 1542 (2010).
[12]H. Kim, B. Truong, J. Buongiorno, and L. W. Hu, Appl. Phys. Lett. **98**, 083121 (2011).
[13]H. S. Ahn, C. Lee, H. Kim, H. J. Jo, S. H. Kang, J. Kim, and M. H. Kim, Nucl. Eng. Des. **240**, 3350 (2010).
[14]R. N. Wenzel, Ind. Eng. Chem. **28**, 988 (1936).
[15]S. G. Kandlikar and M. E. Steinke, Int. J. Heat Mass Transfer **45**, 3771 (2002).

[16]H. S. Ahn, G. Park, J. Kim, and M. H. Kim, Langmuir **28**, 2614 (2012).
[17]H. S. Ahn, H. J. Jo, S. H. Kang, and M. H. Kim, Appl. Phys. Lett. **98**, 071908 (2011).
[18]V. S. Nikolayev, D. Chatain, Y. Garrabos, and D. Beysens, Phys. Rev. Lett. **97**, 184503 (2006).
[19]H. Wang, S. V. Garimella, and J. Y. Murthy, Int. J. Heat Mass Transfer **51**, 6317 (2008).
[20]K. Sefiane, D. Benielli, and A. Steinchen, Colloids Surf., A **142**, 361 (1998).
[21]V. K. Dhir and S. P. Liaw, J. Heat Transfer **111**, 739–746 (1989).
[22]P. J. Berenson, Int. J. Heat Mass Transfer **5**, 985–999 (1962).
[23]A. L. Biance, C. Clanet, and D. Quere, Phys. Fluids **15**, 1632 (2003).
[24]E. Bonaccurso, H. J. Butt, and V. S. J. Craig, Phys. Rev. Lett. **90**, 144501 (2003).
[25]C. Kunert and J. Harting, Phys. Rev. Lett. **99**, 176001 (2007).
[26]C. T. Avedisian and J. Koplik, Int. J. Heat Mass Transfer **30**(2), 379–393 (1987).
[27]E. P. Prokop'ev and S. P. Timoshenkov, Theor. Found. Chem. Eng. **35**(1), 76 (2001).
[28]M. Fatehi and M. Kaviany, Int. J. Heat and Mass Transfer **33**, 983 (1990).
[29]X. Chen and T. D. Papathanasiou, Composites **A37**, 836–846 (2006).
[30]See supplementary material at http://dx.doi.org/10.1063/1.4809944 for visualization results of droplet behaviors on bare (350 °C, 450 °C) and nanotubes (350 °C, 570 °C) surfaces.